MATERIAL-EXTRUSION ADDITIVE MANUFACTURING OF PURE COPPER COMPONENTS FOR ACCELERATOR VACUUM SYSTEMS

A. Hovhannisyan†, A. Davtyan, H. Isunts, V. Yepremyan
Center for the Advancement of Natural Discoveries using Light Emission, Yerevan, Armenia

Abstract

This report presents a carried out study of the technology and performance of three-dimensional printing for the production of parts intended for ultra-high-vacuum assemblies. The simple part geometry was taken as the reference sample. Computer-aided design and finite element method (FEM) analysis are employed to predict thermomechanical stresses and deformations at the sintering stage. Experiments were conducted, and a comparative analysis was carried out to fit the initial FEM results with the experimental ones to obtain actual mathematical models for further simulations. During the printing process, the influence of layer thickness, nozzle temperature, and printing speed on the final density, dimensional accuracy, and surface quality is systematically investigated. Using the given essential parameters new printing setup was developed to ensure the highest density. New samples were printed with the different hole diameters to assess the actual properties using different accuracy printheads. The above-mentioned research was conducted to obtain the highest density of the printed parts, which will be used to evaluate the probability of the accelerator vacuum systems' fabrication.

INTRODUCTION

Additive manufacturing (AM) has become an increasingly relevant approach for the fabrication of complex engineering components, offering advantages in design flexibility, reduced material waste, and shortened production cycles [1, 2]. In accelerator technology, these capabilities are particularly important, as many components require precise geometries, high structural integrity, and efficient thermal management [3]. Conventional manufacturing methods often limit the realization of such features, especially for parts with complex internal structures [2, 3].

AM enables the production of geometries that are difficult or impractical to achieve using traditional machining, including conformal channels and integrated structures [2, 3]. This is of particular interest for accelerator applications such as vacuum components, beamline elements, and thermally loaded structures [3, 4]. However, the implementation of AM in accelerator systems requires careful evaluation of material properties, dimensional accuracy, and process-induced defects [3, 5].

Among the available AM technologies, Bound Metal Deposition (BMD) represents a material-extrusion approach in which a metal–polymer feedstock is extruded layer-by-layer, followed by debinding and sintering [5, 6]. Systems such as the Studio System™ developed by Desktop Metal allow the fabrication of metal parts without handling loose powders, simplifying operation and improving safety in laboratory environments [6, 7]. At the same time, the sintering stage introduces challenges related to shrinkage, residual stresses, and deformation, which are critical for functional components [5, 8, 9]. Vacuum components are essential elements in accelerator systems, where mechanical stability, material homogeneity, and dimensional precision directly influence performance [10]. The application of AM to such components requires not only geometric feasibility but also a detailed understanding of material behavior during thermal processing and the resulting microstructure [5, 8, 10].

In this work, a copper vacuum pipe with a KF flange [11] on one end and a closed opposite side was fabricated using BMD technology. The sintering process was analyzed using finite element simulations performed in SIMULIA ABAQUS to evaluate stress evolution and thermal deformation during heating and cooling [12]. In addition, microstructural investigations were carried out using a metallographic microscope to assess grain morphology, inter-layer bonding, and porosity for samples produced with different printing parameters [13].

The objective of this study is to assess the applicability of BMD-fabricated copper components for accelerator vacuum applications by combining numerical simulation and experimental characterization. The results provide insight into the influence of process parameters on structural integrity and support further integration of AM technologies into accelerator engineering practice.

INITIAL DATA OF SIMULATION

The simulation was conducted in SIMULIA ABAQUS 2019 software environment using following physicomechanical and thermal properties Table 1.

- Table 1: Physicomechanical and Thermal Properties

Properties	**Copper**
Density before sintering [g/cc]	5.2
Density after sintering [g/cc]	8.75
Modulus of Elasticity [GPa]	128
Poisson's Ratio	0.35
Expansion Coeff. [1/°C]	17.24E-06
Thermal Conductivity [W/m×K]	401

The plastic properties are also crucial to include in the model for the simulation of its sintering process. Thus, in

* The work was carried out within the framework of the scientific research topics of the "Vacuum Technologies" basic research laboratory at CANDLE SRI.

† hovhannisyan@asls.candle.am

Figure 1, the stress-strain curves are presented for the material.

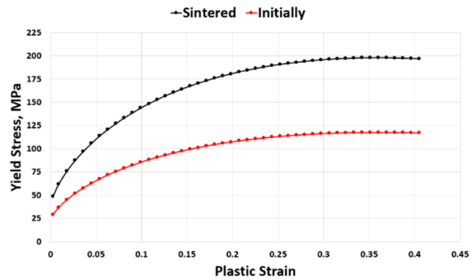

Figure 1: The stress-strain curves for the initial (printed) and sintered materials.

The heating of the part with its further cooling was carried out in stages, as presented in the Fig. 2.

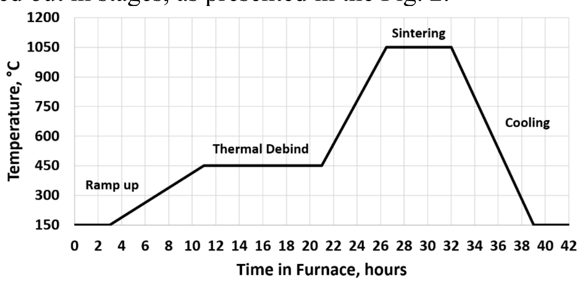

Figure 2: The heating-cooling curve of the sintering process.

SIMULATION RESULTS

The Von Mises stress distribution zones during the sintering process (at 1050 °C), and after cooling (at 20 °C) are demonstrated in Fig. 3.

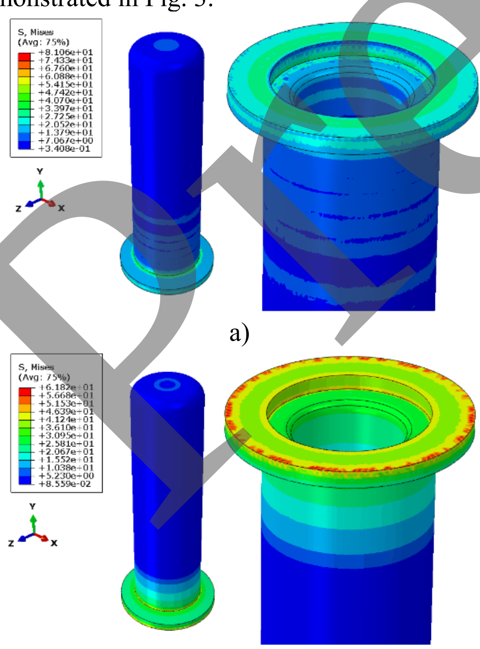

Figure 3: Von Mises stress distribution zones: during sintering (a), and after cooling (b).

In the sintering process (at 1050 °C), the Von Mises stress increased up to 81.06 MPa (Fig. 3a). After further cooling procedure (up to 20 °C), the stress state of the part decreased, and the residual stress of the part reached a maximum of 61.82 MPa (Fig. 3b). The latter is in the KF flange region, because in the tube itself, the maximum residual stress is around 42 MPa near the KF flange, and decreases up to about 1 MPa moving away from the flange (Fig. 3b).

Before reaching the sintering temperature (up to about 900–1050 °C), the part undergoes thermal expan-sion, which is up to approximately 0.258 mm in radial direction and up to about 2.08 mm in length (Fig. 4).

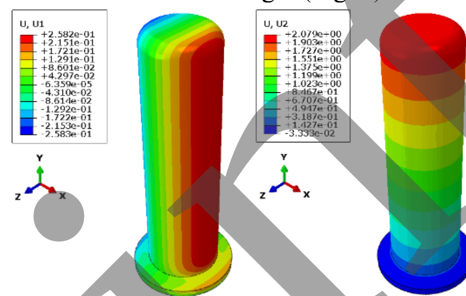

a) b)

Figure 4: The thermal displacement distribution zones before reaching sintering temperature: in radial (a), and longitudinal (b) directions.

MICROSCOPY ANALYSIS

To evaluate the microstructural characteristics of the printed parts, metallographic microscopy investigations were carried out on samples fabricated using different printing parameters. The analysis focused on grain (granule) morphology, inter-layer bonding, and porosity, which are critical factors affecting density and suitability for ultra-high vacuum applications.

The samples were produced using BMD with two standard printhead diameters: 400 µm and 250 µm, as well as an additional high-resolution configuration based on modified printing parameters. A representative view of the printed and debinded copper vacuum pipe with a KF flange, produced using BMD technology, is shown in Fig. 5.

Figure 5: Additively manufactured copper vacuum pipe.

The 400 µm printhead was used with a layer height of 0.20 mm, line width of 0.40 mm, printing speed of 15 mm/s, infill speed of 15 mm/s, and nozzle temperature of 175 °C. The standard 250 µm printhead configuration used a layer height of 0.10 mm, line width of 0.30 mm, printing speed of 15 mm/s, infill speed of 15 mm/s, and nozzle temperature of 165 °C.

An additional sample was fabricated using the 250 μm printhead with modified parameters aimed at improving surface quality: layer height of 0.05 mm, line width of 0.13 mm, printing speed of 10 mm/s, infill speed of 10 mm/s, and nozzle temperature of 165 °C.

Microscopy observations were performed at 400× magnification. Representative images of the asprinted samples produced with the 400 μm printhead are shown in Fig. 6, where grain (granule) morphology and inter-layer gaps are presented, respectively.

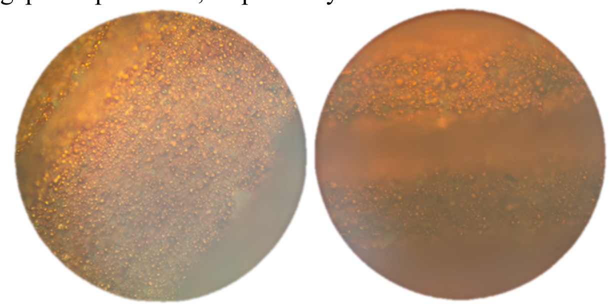

a) b)

Figure 6: Metallographic microscopy images of the sample printed with a 400 μm printhead: grain morphology (a), inter-layer gap (b).

The analysis of these samples shows a non-uniform grain distribution, with granule sizes ranging from approximately 2.5 μm to 12.5 μm. The majority of grains are concentrated near the lower bound, while larger grains appear sporadically. The structure is characterized by low homogeneity, and the inter-layer gap is measured to be approximately 75 μm.

In contrast, the samples printed with the standard 250 μm printhead configuration exhibit significantly improved structural uniformity, as shown in Figure 7.

a) b)

Figure 7: Metallographic microscopy images of the sample printed with a 250 μm printhead: grain morphology (a), inter-layer gap (b).

For these samples, grain sizes range from approximately 2 μm to 10 μm, with a predominantly fine and uniform distribution. The inter-layer gap is reduced to approximately 25 μm, indicating improved inter-layer bonding and reduced porosity.

The additional high-resolution sample printed with modi-fied parameters (reduced layer height and line width) was expected to further improve surface quality and structur-al homogeneity. However, microscopy analysis revealed the opposite trend. The grain size distribution ranges from approximately 2.5 μm up to 14 μm, with a significant fraction of larger grains (12.5–14 μm). The structure is characterized by poor homogeneity, with irregular grain distribution and increased variability compared to the standard 250 μm configuration. This result indicates that excessive reduction of layer thickness and line width, combined with lower printing speeds, may lead to instability in material deposition, resulting in non-uniform packing and deterioration of microstructural quality. Post-sintering data for samples printed with the 400 μm printhead indicate that the inter-layer gap increases to approximately 85 μm. Although microscopy images are not presented for this condition, this behavior can be attributed to shrinkage effects and non-uniform densification during the sintering process.

Overall, the microscopy analysis demonstrates that printing resolution and parameter selection have a strong influence on microstructural quality. While reducing printhead diameter improves homogeneity and inter-layer bonding, further reduction of layer thickness beyond an optimal range may negatively affect structural uniformity. These findings are critical for optimizing process parameters to achieve high-density components suitable for accelerator vacuum applications.

CONCLUSION

The applicability of BMD technology for the fabrication of copper components intended for accelerator ultra-high vacuum applications was investigated. Finite element analysis of the sintering process showed that the maximum Von Mises stress reaches 81.06 MPa at 1050 °C and decreases to 61.82 MPa after cooling, with stress concentration in the KF flange region. Thermal expansion prior to sintering leads to dimensional changes up to 0.258 mm in the radial direction and 2.08 mm in length. Microscopy analysis revealed a strong dependence of microstructural quality on printing parameters. The use of a 250 μm printhead resulted in improved homogeneity, with grain sizes in the range of 2–10 μm and reduced inter-layer gaps of approximately 25 μm. In contrast, the 400 μm printhead produced a less homogeneous structure with grain sizes of 2.5–12.5 μm and inter-layer gaps of about 75 μm, increasing to 85 μm after sintering. It is also shown that excessive reduction of layer thickness and line width leads to deterioration of homogeneity and unstable material deposition. The obtained results confirm that optimization of printing parameters is critical for achieving high-density parts and demonstrate the potential of BMD technology for accelerator vacuum applications. Further work will be focused on improving densification and evaluating vacuum compatibility of the produced components.

REFERENCES

[1] ISO/ASTM, ISO/ASTM 52900:2021 — Additive manufacturing — General principles — Fundamentals and vocabulary, 2nd ed., Nov. 2021,
https://www.iso.org/standard/74514.html

[2] I. Gibson, D. Rosen, B. Stucker, and M. Khorasani, *Additive Manufacturing Technologies*, 3rd ed. Cham, Switzerland: Springer, 2021. doi:10.1007/978-3-030-56127-7

[3] T. Romano, *et al.*, "Metal additive manufacturing for particle accelerator applications," *Phys. Rev. Accel. Beams*, vol. 27, p. 054801, 2024.
doi:10.1103/PhysRevAccelBeams.27.054801

[4] S. Jenzer, *et al.*, "Study of the suitability of 3D printing for ultra-high vacuum applications," in *Proc. IPAC'17*, Copenhagen, Denmark, May 2017, pp. 3356-3358.
doi:10.18429/JACoW-IPAC2017-WEPVA043

[5] C. Suwanpreecha and A. Manonukul, "A review on material extrusion additive manufacturing of metal and how it compares with metal injection moulding," *Metals*, vol. 12, no. 3, p. 429, 2022. doi:10.3390/met12030429

[6] Henry Royce Institute, "Bound Metal Deposition System," accessed Mar. 30, 2026.
https://www.royce.ac.uk/equipment-and-facilities/bound-metal-depositiontm/

[7] Desktop Metal, "Deep Dive: Bound Metal Deposition (BMD)," accessed Mar. 30, 2026.
https://www.desktopmetal.com/article/deep-dive-bound-metal-deposition/

[8] F. Gözüküçük, *et al.*, "Sintering simulation and validation for the sinter-based fused filament fabrication process route," *Prog. Addit. Manuf.*, vol. 10, pp. 10091-10109, 2025.
doi:10.1007/s40964-025-01229-8

[9] J. Jacob, D. Pejak Simunec, A. E. Z. Kandjani, A. Trinchi, and A. Sola, "A review of fused filament fabrication of metal parts (metal FFF): Current developments and future challenges," *Technologies*, vol. 12, no. 12, p. 267, 2024.
doi:10.3390/technologies12120267

[10] V. Baglin and R. Kersevan, "Vacuum systems," *CERN Yellow Rep. School Proc.*, no. 3, pp. 1259-1338, 2024.
doi:10.23730/CYRSP-2024-003.1259

[11] ISO, *ISO 2861:2020 — Vacuum technology — Dimensions of clamped-type quick-release couplings*, 2nd ed., Feb. 2020. https://www.iso.org/standard/79409.html

[12] Dassault Systèmes, "Abaqus finite element analysis," accessed Mar. 30, 2026.

[13] G. F. Vander Voort, Ed., *Metallography and Microstructures*, ASM Handbook, vol. 9. ASM International, 2004. doi:10.31399/asm.hb.v09.9781627081771